10/10-13-91 9:50

SLAC-PUB--5294

DE92 004715

OBSERVATION AND ANALYSIS OF OSCILLATIONS IN LINEAR ACCELERATORS*

John T. Seeman

Stanford Linear Accelerator Center

Stanford University

Stanford, California, 94309

Contents:

* Work supported by Department of Energy contract DE-AC03-76SF00515.

Invited talk presented at the US Particle Accelerator School, Upton, New York, July 24 - August 4, 1989

Also contributed to "The Physics of Particle Accelerators", M. Month, ed., AIP Proceedings (1991)

Conf-890786--4

OBSERVATION AND ANALYSIS OF OSCILLATIONS IN LINEAR ACCELERATORS

John T. Seeman
Stanford Linear Accelerator Center
Stanford, California 94309

I. INTRODUCTION

All particles in accelerators exhibit oscillations of some form about so called nominal parameters responding to internal and external forces. Most forces try to contain the beam within a specified (six dimensional) phase space volume to provide acceptable beam properties at its destination or to provide for good transmission. Other forces try to enlarge the phase space volume. The containment of a beam within the desired phase space volume depends upon many dynamic effects including initial phase space volumes or emittances, internal energy spectra, acceleration, focusing, steering, and component and alignment errors. Effects from space charge and short and long range wakefields are also important. The analysis of an oscillation involves not only understanding the transport equations of the beam but also the measurement techniques, the beam environment, and any possible accelerator errors that may affect beam motion. A good diagnosis of actual beam oscillations in an accelerator leads to a more complete understanding of the accelerator and towards more optimal accelerator performance.

The analysis of oscillations, in general, involves the measurement of beam parameters followed by comparison with predictions to infer internal bunch properties. Measurements are taken with instruments which may interfere with the beam as it passes or may let the beam pass undisturbed. As examples, transverse profile monitors often intercept the beam changing its profile downstream, whereas position monitors usually do not affect the beam. Always, the measurements represent projections of the particle distributions onto fewer than six dimensions (two or less). Often, the projection reveals the bunch quantity of interest but frequently measurements of several different projections are needed to unfold the appropriate beam distribution. A prediction of beam properties can be made knowing the configuration of the accelerator

components and the on line set point values used during the measurements. Errors in the measurements and in the set points are often compounded by unknown internal errors in the accelerator, such as associated with magnet alignment, acceleration gradients, vacuum chambers, or power supply ripple. The art of experimental accelerator physics is in the choice of the appropriate measurements and machine model with explicit errors so that the prediction and measurements illuminates the appropriate physical issue. Thus, the study of oscillations is usually an inverse problem where the input parameters and the output values are reasonably well understood but the physical process in-between is to be determined [1].

An experimental accelerator physicist struggling with inverse problems may conclude the following:

Axiom 1: *If a mode of oscillation is physical possible for a beam, nature tends to provide a stimulus to excite that oscillation.*

Axiom 2: *When a previously unobserved beam dynamics effect is measured for the first time, the likely outcomes with decreasing probability are:*

1) *The measurement instrument has malfunctioned (hardware, software, or user errors).*
2) *The instrument measured a secondary effect (cross-talk, feed-through, or saturation).*
3) *An ordinary physics effect has been interpreted as a more complicated effect (shape, tails, jitter, averaging, or scrapping).*
4) *A new accelerator physics effect has been discovered (publish).*

Desire usually ranks them in reverse.

Furthermore, independent or redundant measurements help a great deal in distinguishing misinformation from useful accelerator physics. The ability to distinguish and verify useful information from misinformation is often the difference between rapid progress and misguided efforts. Therefore, strong skepticism of the interpretation of measurements and predictions is often warranted.

One intent of this article is to emphasize effects which occur over many betatron wavelengths (10 to 100 oscillations) or in an open ended system. Accelerators in this

category include linear colliders, long transport lines, and, to a certain degree, synchrotrons and single-pass injector chains. Examples from several accelerators are shown, mainly from the Stanford Linear Collider (SLC) [2,3]. Effects occurring within a few betatron wavelengths are covered here but have been discussed in greater detail elsewhere [4,5,6]. Effects which occur in circular accelerators (storage rings) that have beam orbits closing on themselves and come to equilibria have been studied extensively elsewhere [7,8,9,10,11] and are not covered.

1.1 List of Variables

s	Longitudinal distance along the accelerator or transport line.
t	Time.
z	Longitudinal distance within a bunch.
x (y)	Horizontal (vertical) position of a single particle relative to the nominal trajectory.
x' (y')	Horizontal (vertical) angle of a single particle relative to the nominal trajectory.
λ_β	Betatron wavelength.
ψ	Betatron phase advance.
β,α,γ	Twiss parameters ($\beta\gamma = 1+\alpha^2$).
R_{ij}	First order transport matrix between two longitudinal positions.
T_{ijk}	Second order transport matrix.
σ_x, σ_y	Horizontal (vertical) beam size.
σ_z	Longitudinal bunch length.
E	Beam energy.
ΔE	Deviation of the average beam energy from the nominal.
σ_E/E	Energy spectrum of the beam.
δ	Fractional energy deviation of a particle $\Delta E/E_0$.
σ_{ij}	Components of the beam 'sigma' matrix.
$\gamma\epsilon$	Invariant beam emittance ($\gamma = E / m_e c^2$).
η,η'	Dispersion functions.
k	Lattice spatial frequency ($2\pi / \lambda_\beta$).
r_e	Classical radius of the electron.

1.2 Definition of Phase Space

The state of an arbitrary particle at a longitudinal position s along an accelerator can be represented using a vector X(s).

$$X(s) = (x,x',y,y',z,\delta)^T \tag{1}$$

The state of that particle at another position s_f is obtained by matrix multiplication of the initial vector with all the n transport components in between.

$$X(s_f) = R(n)R(n-1) \ldots R(3)R(2)R(1)\, X(s_0) = R(s_f, s_0)\, X(s_0) \tag{2}$$

Each transport element has a well determined 6 X 6 dimensional transport matrix R. This representation is only the first term of an expansion. The second order may be represented by the T matrix [5]. Knowledge of the R and T matrices for all elements completely describes the transport system (to second order).

$$X_i(s_f) = \sum_j R_{ij} X_j(s_0) + \sum_{jk} T_{ijk} X_j(s_0) X_k(s_0) \tag{3}$$

In systems with periodic arrays of elements, which includes most modern accelerators and long transport lines, it is convenient to describe the transport in terms of Twiss parameters. The Twiss parameters are not as uniquely defined as the R and T matrices as arbitrary initial conditions must be specified. The advantage of using Twiss parameters is in the ease at which they can be applied in day-to-day activities. The definitions of the Twiss parameters are shown in Figure 1. Given a plot of the betatron function along the accelerator and the beam emittance, one can calculate very quickly the approximate trajectory resulting from changed dipoles, the sensitivity to dipole errors, the expected beam size at any location, or identifying locations of difficult matching conditions [11]. The less convenient alternative is to know the R matrices from all points to all others. The confusion with the Twiss parameters enters during the discussion of lattice parameters and beam parameters. The quadrupole lattice is designed with specified input Twiss parameters. The beam, however, enters the transport line with different input conditions and with have its own betatron functions along the accelerator.

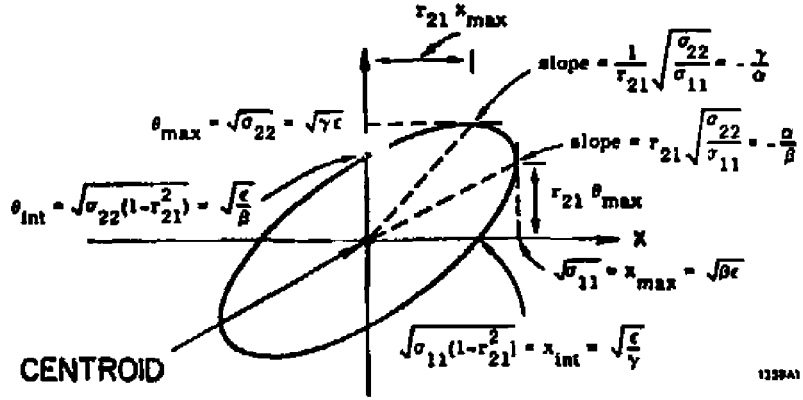

Figure 1 Phase space coordinates defining the Twiss parameters.

The lattice Twiss parameters can be obtained from the R matrix for a matched cell [7].

$$\begin{aligned} \cos(\psi) &= (R_{11} + R_{22})/2. \\ \beta &= R_{12}/\sin(\psi). \\ \gamma &= -R_{21}/\sin(\psi) \\ \alpha &= (R_{11} - R_{22})/2\sin(\psi) \end{aligned} \tag{4}$$

2. BETATRON OSCILLATIONS

The positions of the beam along the accelerator are measured with position monitors, an example of which is shown in Figure 2. A position monitor measures the average center position of the beam. A system of these monitors can be used to study the beam positions along an accelerator. A typical trajectory of a single electron bunch in the SLC is shown in Figure 3 including a betatron oscillation. The lattice Twiss parameters for the first 150 m of the SLC linac are shown in Figure 4. As with most as-built accelerators the periodic cells are interrupted with transitions. Note the change

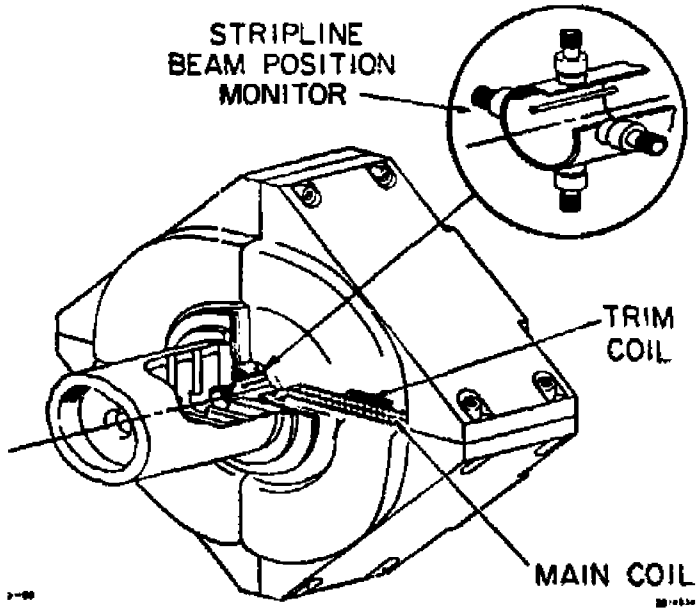

Figure 2 Schematic view of a strip line beam position monitor.

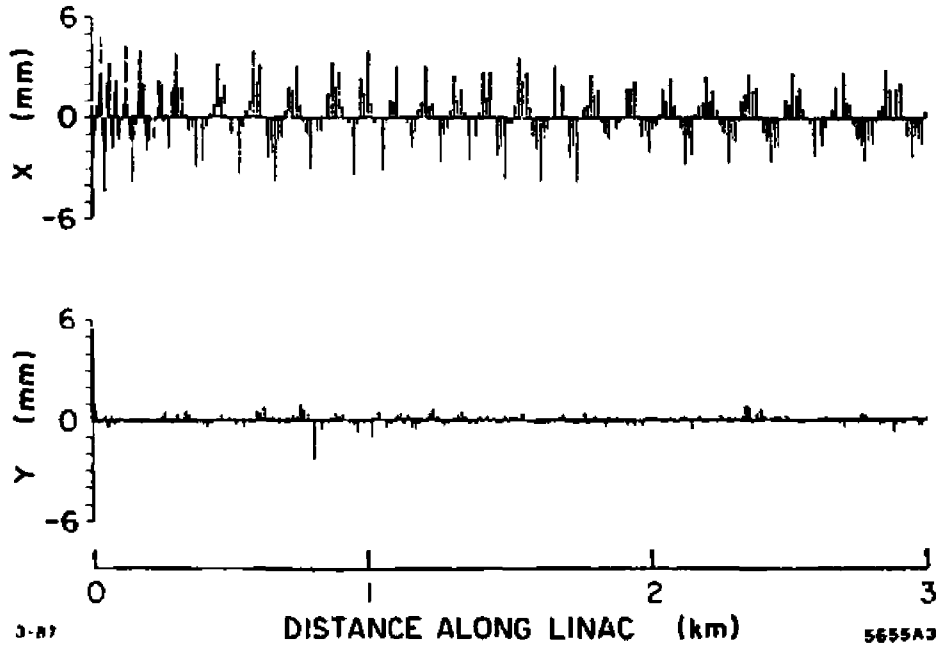

Figure 3 Observed betatron oscillation in the SLC linac induced by a horizontal dipole change near the beginning. From small quadrupole roll errors, a small oscillation is coupled in, then out, of the vertical plane in the region 600 to 1200 m.

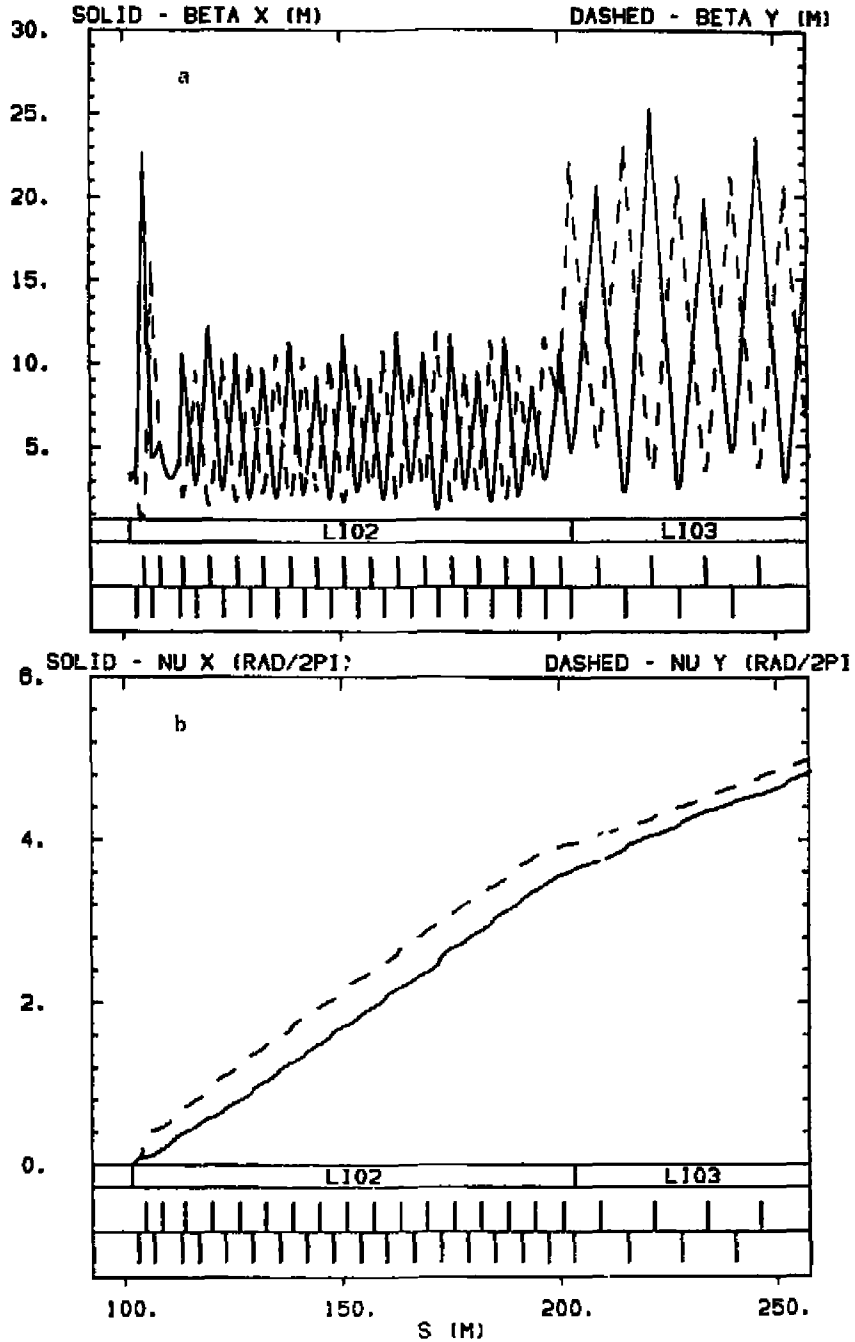

Figure 4a,4b Plots of the betatron functions and phase advances for the first 150 m of the SLC Linac.

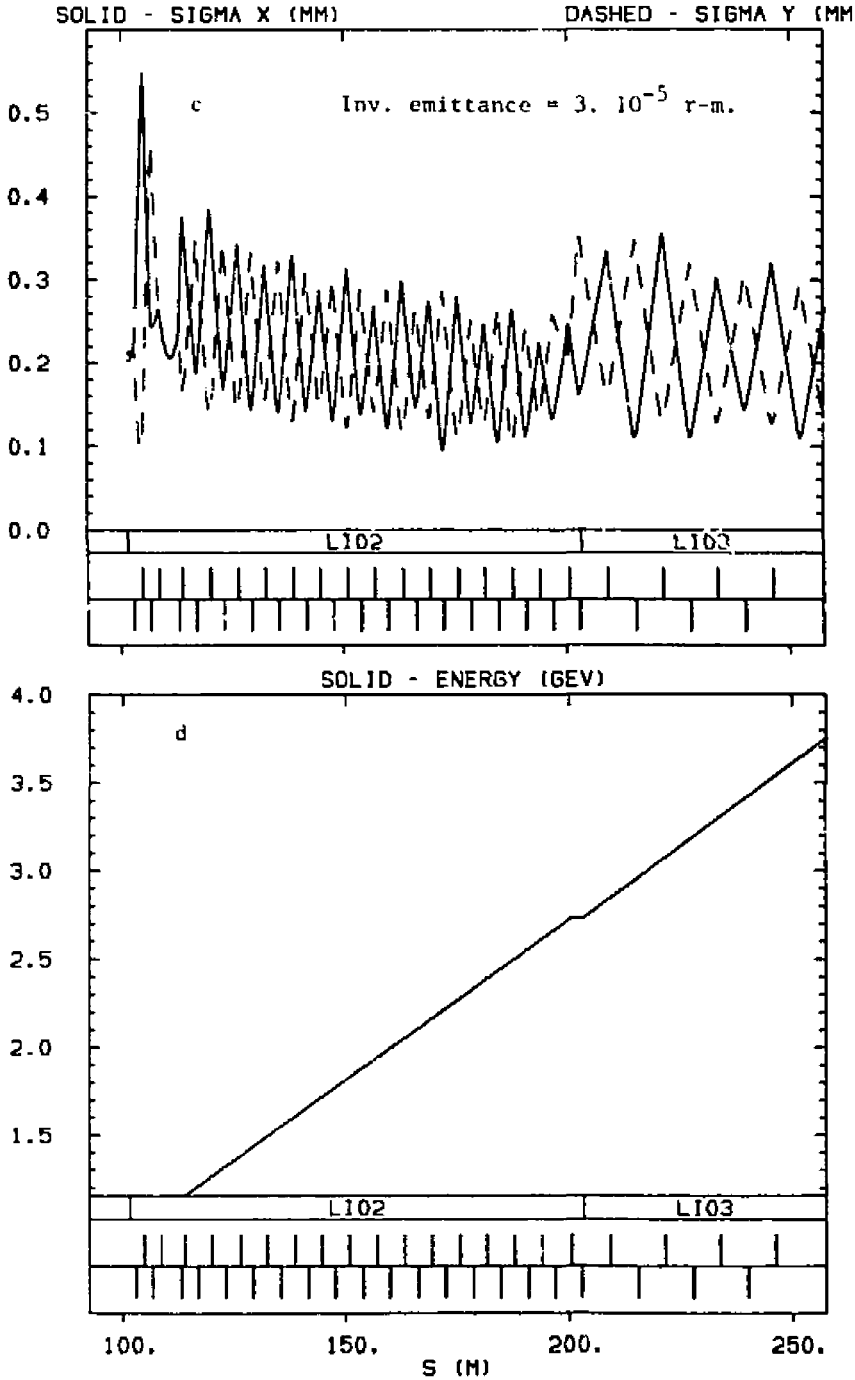

Figure 4c,4d Plots of the beam sizes and energy profile over the first 150 m.

in the quadrupole spacing at 210 m and also the $\beta_x = \beta_y$ region for a spin rotator at 110 m in Figure 4. The expected beam oscillation given a dipole deflection $\Delta\theta$ at location '0' with acceleration is

$$x(s) = \Delta\theta\ \beta(s)\sqrt{E(0)\ \beta(0)\ /E(s)\ \beta(s)}\ \sin(\psi(s)-\psi(0)) \qquad (5)$$

2.1 Measurement and Analysis of a Betatron Oscillation

A fit can be made to an observed betatron oscillation using Eqn. (5). Two examples are shown in Figure 5. Short range fits (Figure 5a) are typically used for feedback systems and long range fits (Figure 5b) are useful for lattice checks [12]. Many measurements per betatron wavelength make the analysis robust against errors. A least-squares fitting algorithm is usually effective. The fits can vary several parameters, for example the initial amplitude, the overall energy scale, or quadrupole errors.

2.2 Identification of Errors using Oscillations

Betatron oscillations are useful in diagnosing errors in an accelerator. A comparison of an actual lattice to a theoretical design can be made using a single fit parameter: the initial amplitude. In Figure 6 a measured oscillation with an amplitude fit over the first two wavelengths shows that the accelerator conditions match the design over 25 wavelengths. In Figure 7 the same analysis shows that at a different time the accelerator lattice has errors downstream. Corrections are then in order. In Figure 8 lattice checks are used to determine that a klystron has been misphased and indicates within two or three klystrons out of 230 which is at fault [13].

By making a deliberate oscillation with an accelerator component and comparing it to an observed undesired change in the beam, one can determine candidates for in depth investigations of the source. See Figure 9.

Position monitors usually measure both the horizontal and vertical position simultaneously. Thus, an observation of an oscillation can be used to determine

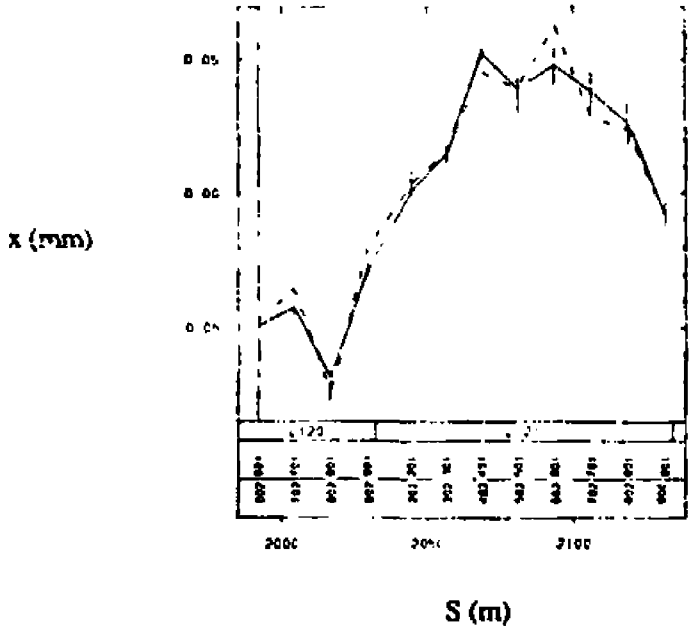

Figure 5a Measured betatron oscillation over about one wavelength. The fit (dashed line) agrees well with the data (solid line). A single position monitor reading is accurate to about 13 microns (average of 5 readings) but the fit is good to about 5 microns. Thus, averaging and fitting improves the definition of a betatron oscillation significantly.

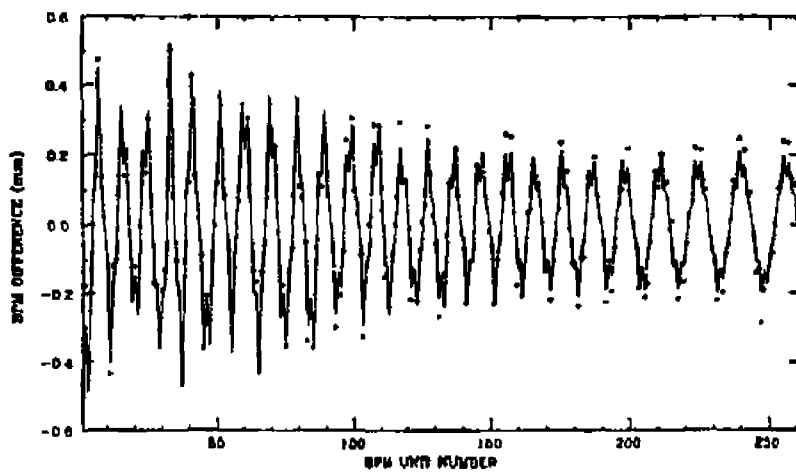

Figure 5b Measured oscillation along the entire linac. The data (points) can be fit quite nicely with a model (solid) having a single adjustable energy scale over the linac. The energy scale is adjusted by a few percent.

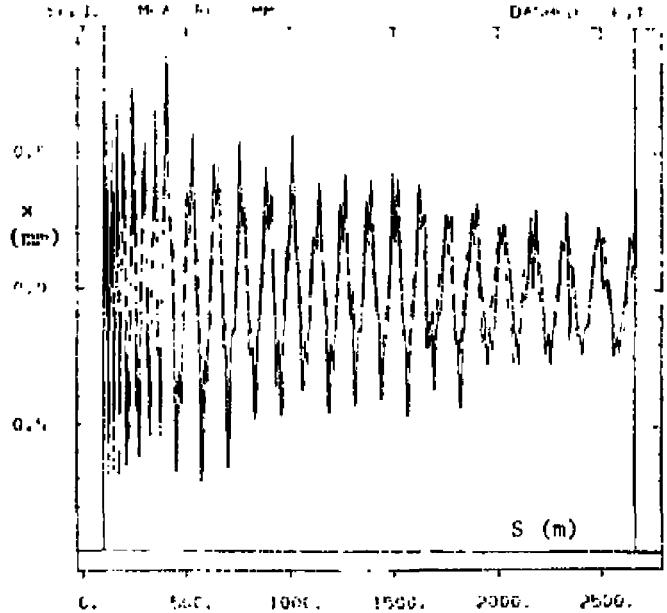

Figure 6 **Measured oscillation and a one parameter amplitude fit showing the predicted trajectory downstream. The agreement is good.**

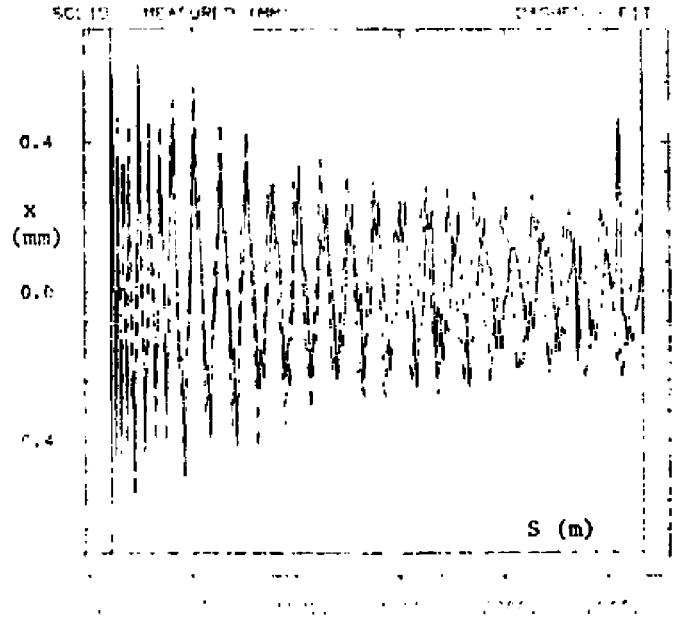

Figure 7 **Measured oscillation and a one parameter amplitude fit showing the predicted trajectory downstream. The oscillation amplitude and betatron phase have gradually growing errors in the second half of the accelerator due to a lattice mismatch and a scale factor error in the quadrupoles.**

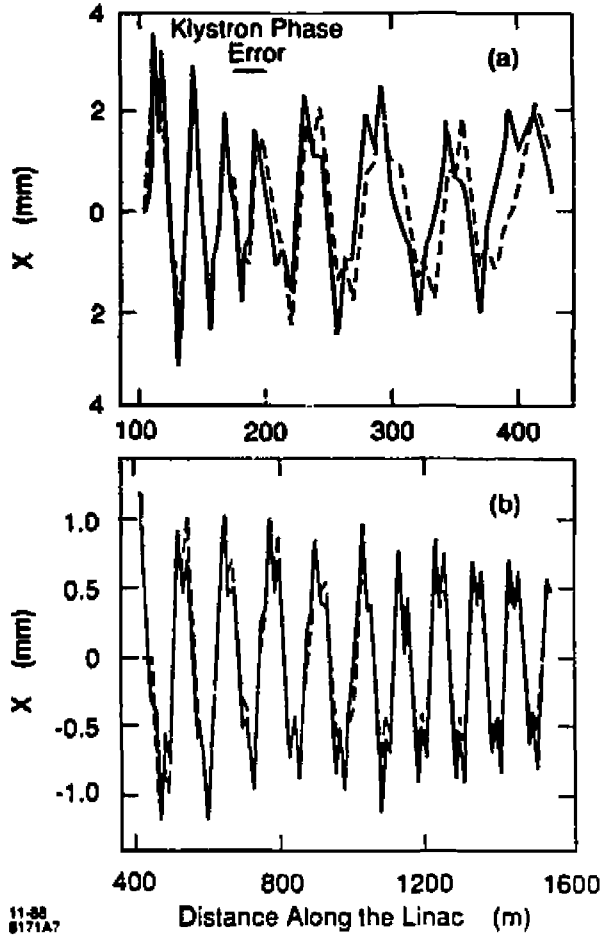

Figure 8

Measured (solid) and predicted (dashed) betatron oscillations. The oscillation in plot (a) had a lattice with a klystron phase error making the beam oscillate too rapidly as its energy was low. After the phase error was fixed, the oscillation agreed with predictions, see plot (b).

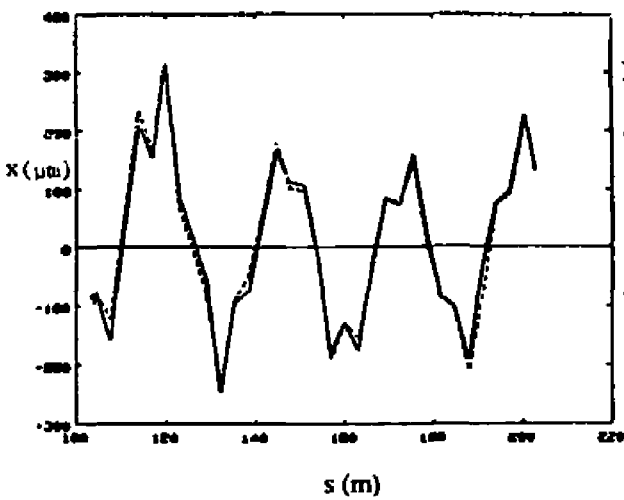

Figure 9

A sudden natural beam change (dashed line) is compared with an induced perturbation (solid line) by changing the damping ring extraction kicker strength. Induced changes such as this one provides strong candidates for error determination.

coupling from one plane to the other. An example of cross plane coupling in the SLC Arcs is shown in Figure 10. Note the minute details that can be extracted from the data [14].

A more complete set of oscillations can be used to investigate further details of a transport system [15]. If the data from two correctors are changed in a grid pattern and readings from several position monitors are recorded, then the linearity of the transport line can be investigated, as is shown in Figure 11. Multiple constraints can then be applied to the data, such as reproducibility or fits to second order fields, to improve the results.

Collimation of the beam to reduce its transverse shape can affect it centroid position. As seen in Figure 12, collimation on one side of the beam shifts the centroid of the beam away from the collimator. The effect is to produce an observed oscillation in the beam downstream where there was none before.

2.3 Effects of the Energy Spectrum on Oscillations

A beam contains many particles which do not have identical energies. The spread in the particle energies within a beam affects observed oscillations. Because of longitudinal wakefields, the internal energy spread can be quite large and have a complicated distribution [16,17]. As the bunch intensity increases, the distribution changes as can be seen in Figure 13. When a bunch receives a dipole kick and then oscillates downstream, the different energy particles oscillate with different frequencies and soon start to filament. In Figure 14 this filamentation process can be seen schematically. The bunch filaments into a annular ring when the low energy and high energy particles relatively slip phase by one cycle. In a standard FODO lattice the amplitudes of oscillation of the various energy particles do not differ very much as the betatron functions vary slowly with energy. But the betatron phase advance per cell changes inversely with energy, determined by the chromaticity of the lattice.

Closed dipole bumps for steering at a nominal energy do not close for off-energy particles and thus generate a position-energy correlation or dispersion.

$$\eta = \Delta x / (\Delta E / E_0). \qquad (6)$$

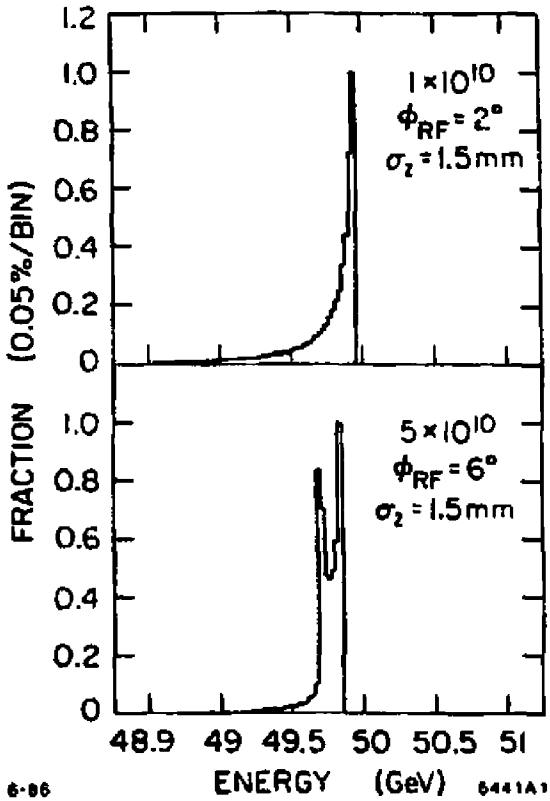

Figure 13 Minimized energy spectra at low and high currents. At high beam currents longitudinal wakefields produce a complicated energy spectrum which is observed in practice. These spectra complicate the transport of low emittance beams.

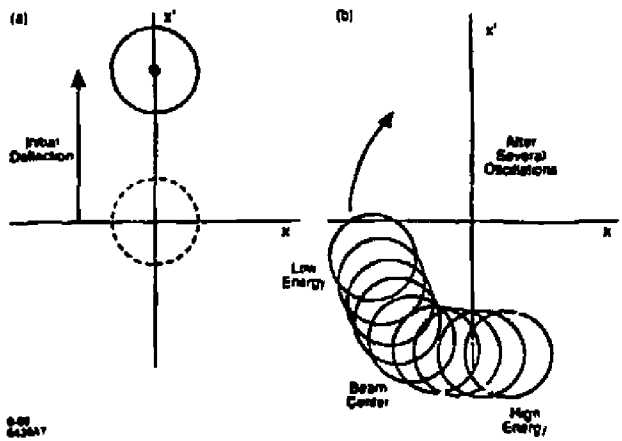

Figure 14 Smearing of a beam from a dipole kick and ensuing betatron oscillation produced by an energy dependent betatron phase advance per cell.

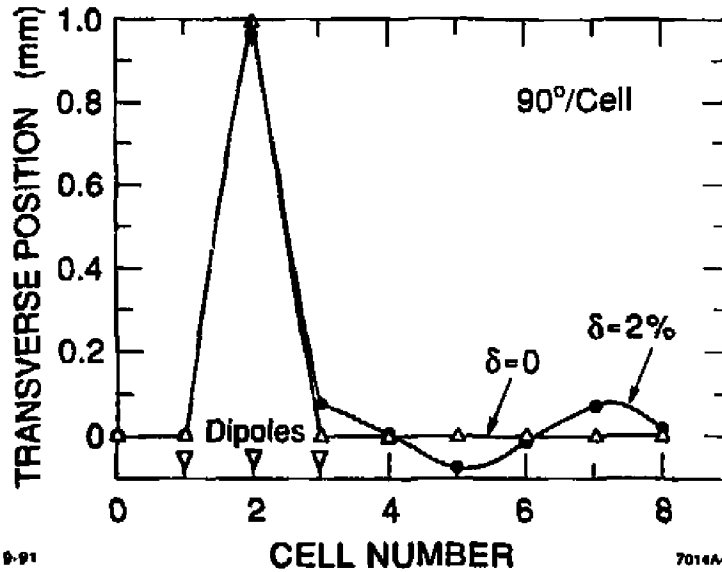

Figure 15a Dispersion is generated from a closed dipole beam bump in a quadrupole lattice. There are two quadrupoles per cell. If the bump is closed for an on-energy particle ($\delta = 0$), then the bump is not closed for off energy particles. Trajectory correction , in general, can be viewed as a series of beam bumps.

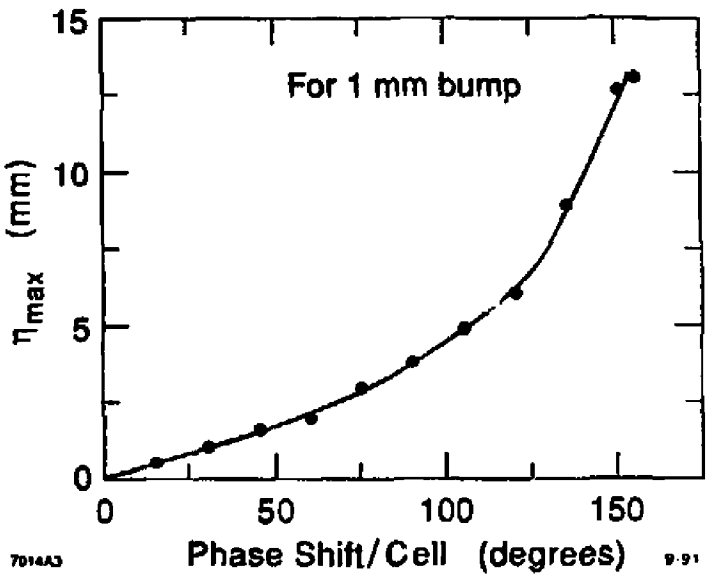

Figure 15b The dispersion generated from a single beam bump as a function of phase advance per cell. The dispersion increases nonlinearity with lattice strength. The bump is closed for all energies with the quadrupoles off.

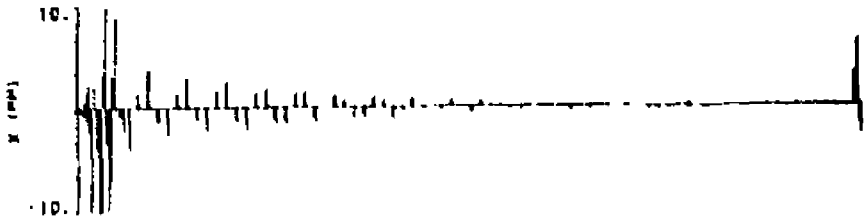

Figure 16 Decoherence of an oscillating positron bunch in the positron return transport line (2 km). The energy spread of the bunch is about 5%.

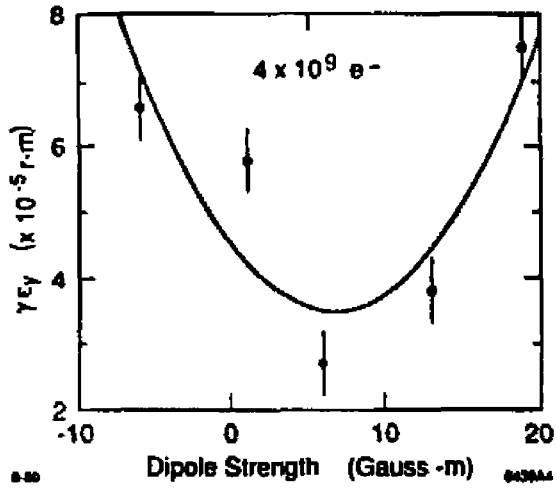

Figure 17 Dispersion increased emittance at 47 GeV with an oscillation starting early in the linac. The low bunch charge makes very small wakefield effects.

$$\frac{d^2}{ds^2} x(z,s) + k^2(z,s)\, x(z,s) = \frac{r_e}{\gamma(z,s)} \int_z^{\infty} dz'\, \rho(z') W_{\perp}(z'-z)\, x(z',s), \qquad (7)$$

where k is the lattice strength, ρ is the longitudinal particle density, and W is the transverse wakefield which depends on the separation of the leading and trailing particles. W grows nearly linearly for most bunches. The driving force on the right hand side is proportional to the transverse offset of the leading particle in the RF structure of the accelerator. Thus, there is the potential for resonant excitation of the back of the bunch by the head. The wakefield excitation of the bunch through an oscillation can be seen schematically in Figure 18. However, there are other mechanisms to start this resonant excitation. For example, a misaligned accelerating structure, as in Figure 19, will excite the core and back of the bunch leaving the head of the bunch on axis. The core of the bunch continues to excite any trailing particles.

A method to control this resonant growth is called BNS damping (named after the inventors: V. Balakin, A. Novokhatsky, and V. Smirnov). BNS damping lowers the energy of the back of the bunch by accelerating the bunch behind the crest of the RF early in the linac and then leading the RF crest downstream to restore the energy spread at the end. With the back of the bunch low in energy, the wakefields forces in Eqn. 7, which act to defocus particles, are counterbalanced by the increased quadrupole focusing of the back of the bunch because of its low energy. The resonant excitation is then reduced. It is not possible to perfectly cancel the forces over the whole bunch so some enlargement is expected.

In the framework of BNS damping it is interesting to observe oscillations as a function of beam current. In Figure 20 are shown oscillations with various intensities and conditions. These oscillations no longer follow damped betatron oscillations with acceleration. Oscillation excitation and beats in the position signals can clearly be seen.

By recording a trajectory and fitting the oscillations using Eqn. 7, an effective beam current (given a gaussian bunch length σ_z) can be calculated. This fitted current versus the actual current for a particular SLC accelerator condition is shown in Figure 21. Although the data and the predictions do not fully agree, there is no doubt about the strong effect on the apparent betatron frequency [20].

Once a bunch has a skew profile it is not possible to correct the bunch with steering to completely remove all transverse wakefield effects. Some of the possible injection conditions of a bunch into an accelerator are shown in Figure 22, indicating the importance of a well corrected and controlled launch. Plot (a) is for a perfect

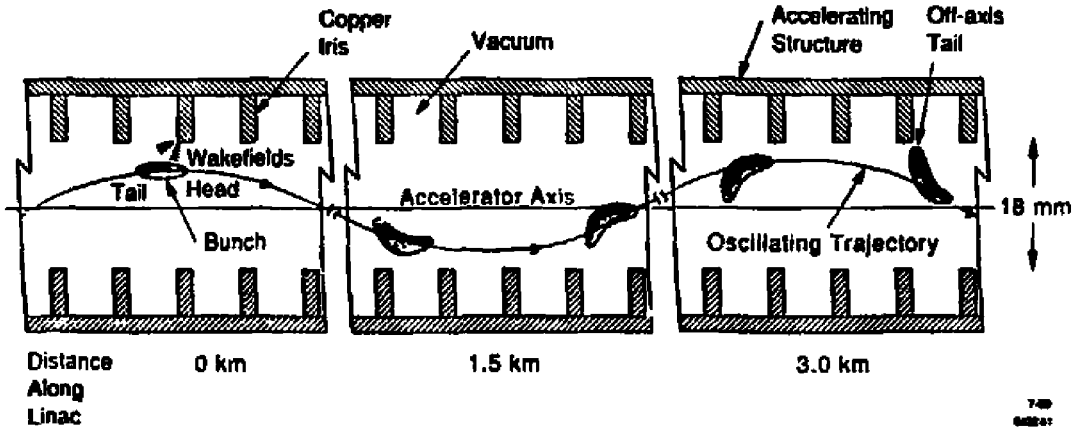

Figure 18 A beam oscillation in an accelerating structure produces head-tail transverse wakefields which distort the transverse bunch profile. Trajectory correction downstream will have difficulty converging as some part of the bunch is always off axis.

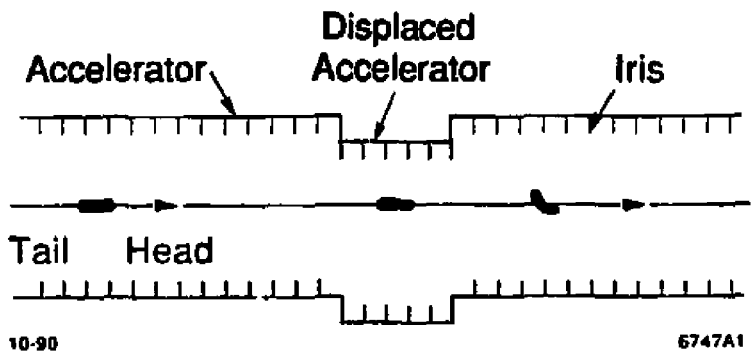

Figure 19 A displaced accelerating structure will induce wakefield distortions in a bunch. Again, trajectory correction will have difficulty correcting the result. There are many of these small distortions (random) in an accelerator and they collectively contribute to the beam shape.

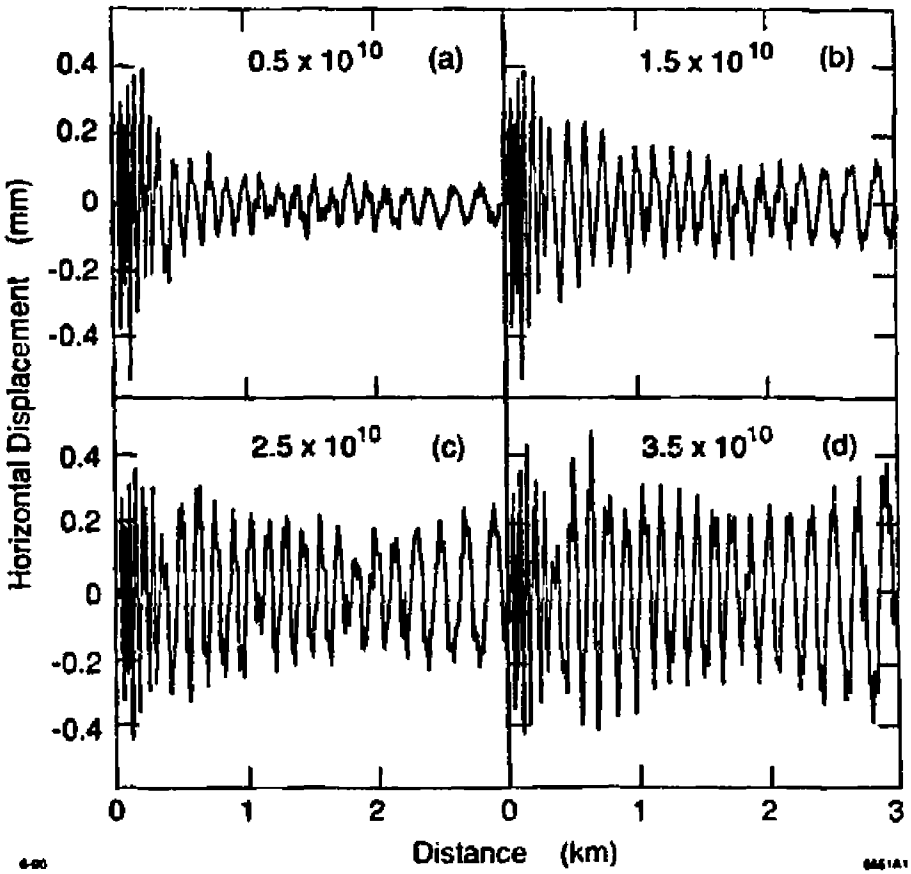

Figure 20a Observed driven single bunch oscillations along the linac versus charge. Standard BNS conditions for 3×10^{10} e^- are used in all cases but with the linac overall phase adjusted to make a small energy spectrum at 47 GeV. Note that at high charge, damping from acceleration is not as strong as wakefield growth in the latter half of the linac.

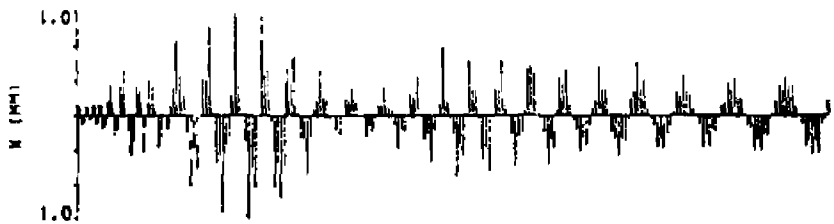

Figure 20b Observed oscillation for a single bunch when the energy spectrum is not properly set along the linac. Apparent trajectory beating can be seen.

bunch, (b) shows a transverse offset, (c) shows a head-tail energy spread and dispersion, (d) indicates upstream wakefields, (e) characterizes second order terms (T_{166} for example), and (f) is similar to (c) but with η' added.

Oscillations can be used to study long range wakefields as shown in Figure 23. Two bunches were made to oscillate along the linac. The trajectory of the second bunch was measured with and without the leading bunch. No noticeable change can be seen for the nominal 60 ns spacing. Effects were seen, however, with a 10 ns spacing.

4. TRANSVERSE PROFILE OSCILLATIONS

Each particle of the beam is transported according to Eqn. 2. The ensemble of particles which makeup the beam can be described in a notation which can be propagated along the transport line using the R matrix. At a location s_0 the beam is described using the 'sigma matrix' Σ which has 21 independent parameters because of symmetry. Each element σ_{ij} of Σ is an average over two variables, $\sigma_{ij} = < x_i\, x_j >$. The beam matrix Σ at s can be obtained from Σ at s_0 using the R matrix from s_0 to s.

$$\Sigma(s) = R\, \Sigma(s_0)\, R^T \tag{8}$$

The beam can also be represented using Twiss parameters which are unique to the beam and not necessarily those of the lattice. This equation describes the changes in the bunch transverse size σ as it is transported along the accelerator.

$$\sigma(s) = [\, \beta(s)\, \varepsilon]^{1/2} \tag{9}$$

4.1 Profile and Emittance Measurements

The profile of the beam is measured with devices that have resolutions small compared to the beam size. As modern day accelerators are producing ever smaller beams, monitoring of beam profiles is now a fine art with new directions needed constantly. Two venerable profile monitors are shown in Figures 24 and 25. Screen monitors are very good at observing fine details of the beam, such as small tails [21]. Wire scanners are very good at surviving high beam currents, at causing minimal program interruption, and having fine resolutions [22].

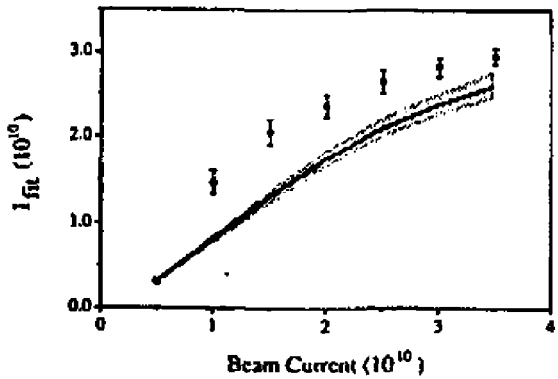

Figure 21 Apparent beam current as determined from betatron oscillations as a function of actual beam current. Transverse wakefields enter the equation of motion for relatively modest currents.

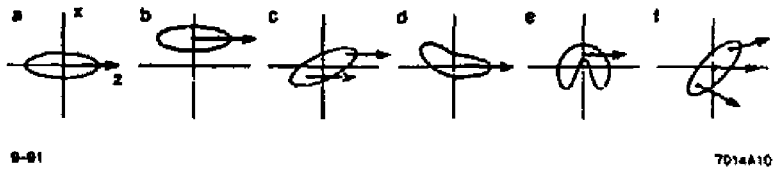

Figure 22 Possible injection orientations of a bunch entering a linac. All orientations have wakefield and dispersion implications except for plot (a), the ideal condition.

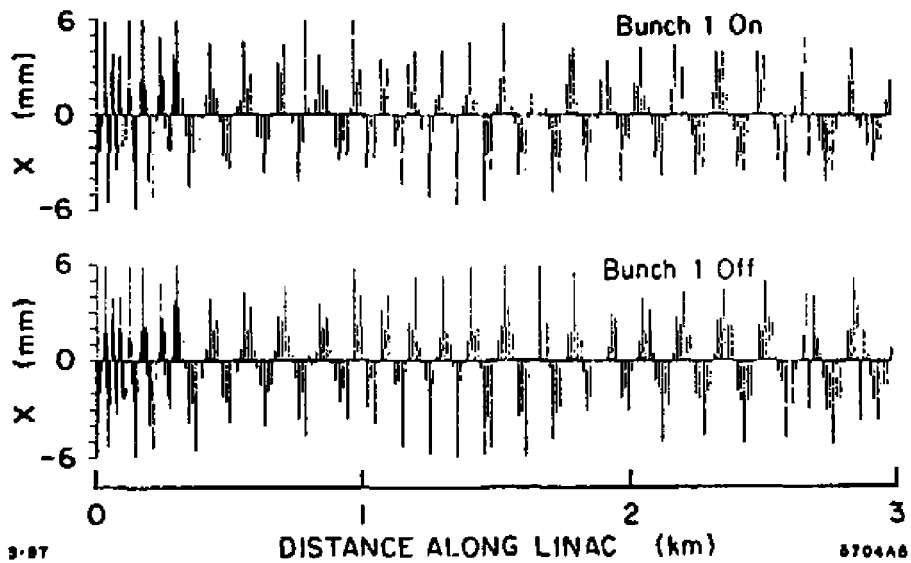

Figure 23 Oscillations of a trailing bunch when the leading bunch is present or not. These studies provide information about long range wakefields.

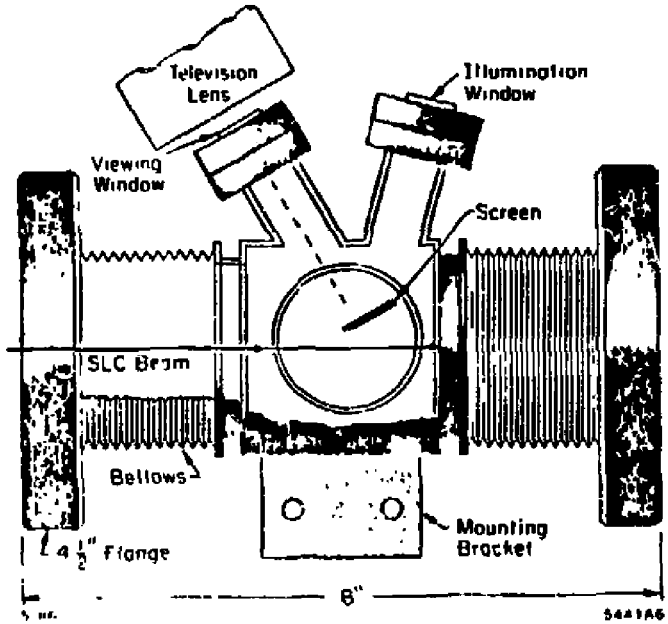

Figure 24 Schematic view of a fluorescent screen profile monitor. The screen is moved into the beam using the flexible bellows. The tilt of the screen increases the resolution in that plane. The camera is tilted by the same angle for depth of focus issues. The resolution can be 20 microns.

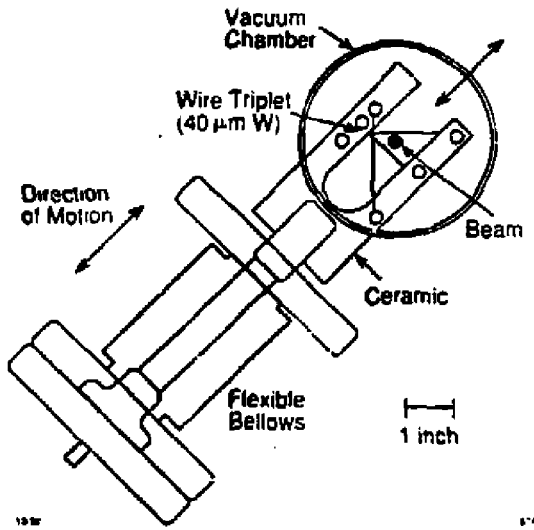

Figure 25 Schematic view of a moving wire profile monitor. Three wires give x, y, and u (45 degrees) profiles on a single scan. The wire is typically gold plated tungsten 40 microns in diameter. The resolution of a measured 200 micron diameter beam is about 3-10 microns.

Two typical beam profiles are shown in Figure 26 displaying digitization and computer fitting algorithms now available from industry. Software applications are also quite sophisticated [23]. The emittance of the beam can easily be measured (see Figure 27). With automatic measurement software, emittances and beam Twiss parameters can be measured every few minutes if desired without intervention [24].

4.2 Profile Changes from Betatron Errors

If the betatron functions of the beam are matched to the lattice, the beam is transported without enlargement. With mismatched betatron functions, the beam size undergoes size oscillations along the accelerator beyond those given by the undulating $\beta(s)$. This process can be seen in Figure 28. Filamentation occurs as the beam tumbles downstream. Eventually, the beam rematches to the lattice betatron functions but with a larger emittance, as shown in Figure 29. The increased emittance is given by a factor labeled Bmag [25].

$$(\gamma\varepsilon)_{final} = \text{Bmag}\,(\gamma\varepsilon)_{initial} \tag{10}$$

with

$$\text{Bmag} = \frac{1}{2}\left[\frac{\beta_l}{\beta_b} + \frac{\beta_b}{\beta_l} + \beta_b\,\beta_l\left(\frac{\alpha_b}{\beta_b} - \frac{\alpha_l}{\beta_l}\right)^2\right] \tag{11}$$

where l refers to the lattice and b refers to the beam, both determined where the mismatch occurred. To avoid emittance increases of order 10%, β must be matched to 30% or so. The α match has a similar constraint.

Several nonlinear effects can also induce profile oscillations. First, similar to Figure 12, a collimator directly affects the shape of the beam and, thus, the effective emittance and betatron functions derived from beam measurements. This can be seen in Figure 30. Because of filamentation from the internal energy spread of the beam, the collimated phase space can repopulate if allowed. Secondly, higher order fields in transport magnets often affect the outer regions of a population of particles in phase space and significantly change their density [26]. An example is shown in Figure 31. These density changes can be measured by changing the oscillation phase relative to the profile monitor location (typically using the beam energy).

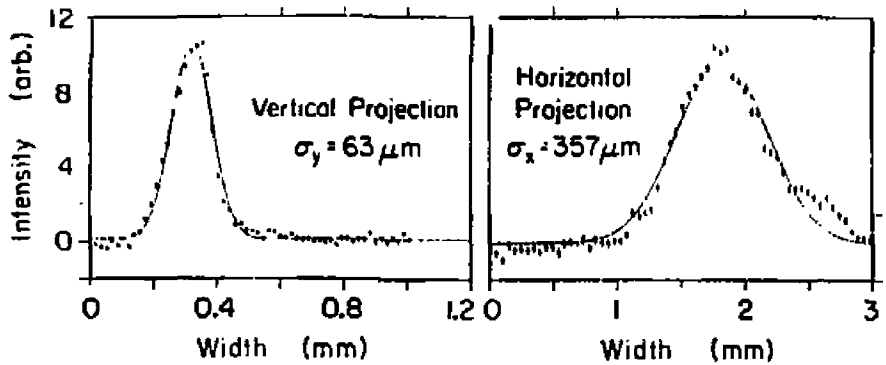

Figure 26 **Typical measurements of vertical and horizontal beam sizes. A Gaussian fit has been performed on the data. Non-Gaussian beam shapes can affect the fitting process. Screen profile monitors can measure a beam shape on a single accelerator pulse. Wire scanners require many pulses or many wires.**

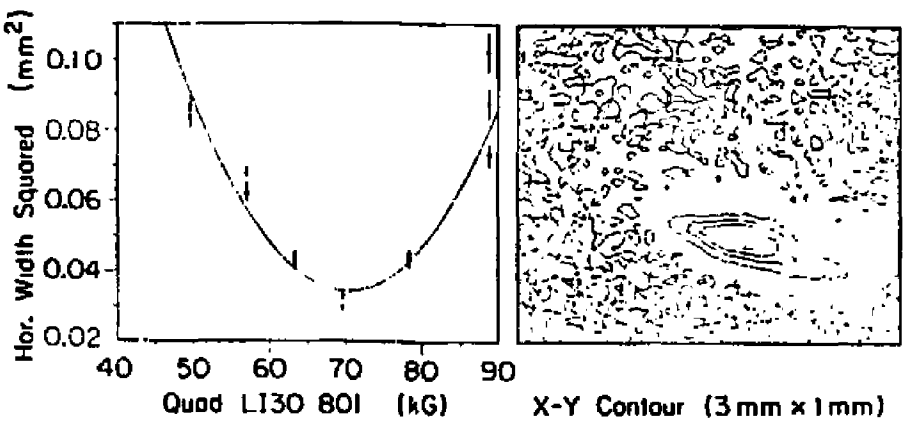

Figure 27 **A determination of the beam emittance is made by measuring the beam size on a profile monitor as a function of the strength of an upstream quadrupole. The x-y beam skew can be determined from contour plots. The emittance can also be determined by measuring the beam size at three or more distinct betatron phase locations. Wire scanners at several locations are convenient for these measurements as they can be designed to minimize any interruption to the program.**

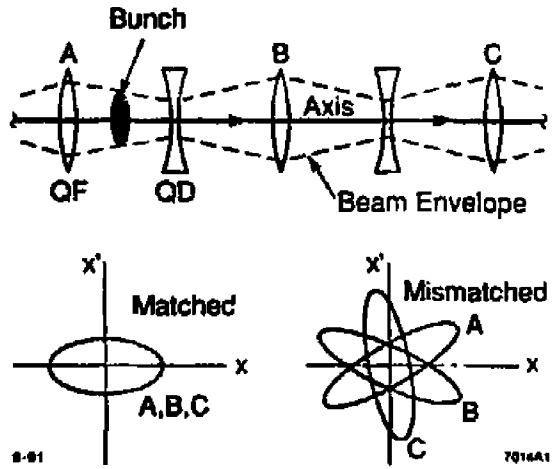

Figure 28 A beam that is matched to a periodic lattice will have the same phase space orientation at all equivalent locations, e.g. points A, B, and C. A mismatched beam will have a phase space orientation which changes from one equivalent location to the next.

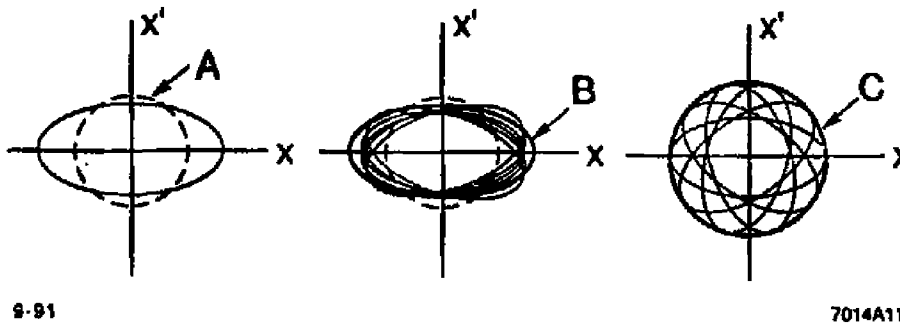

Figure 29 A mismatched beam will filament because of its internal energy spread. Initially, as in diagram"A", the beam betatron function is mismatched but the emittance is unchanged. As the beam starts to filament, as in diagram "B", the effective beam betatron function begins to return to the matched value but the emittance increases. After full filamentation, as in diagram "C", the betatron function of the beam returns to the matched value and the growth of the beam emittance stops.

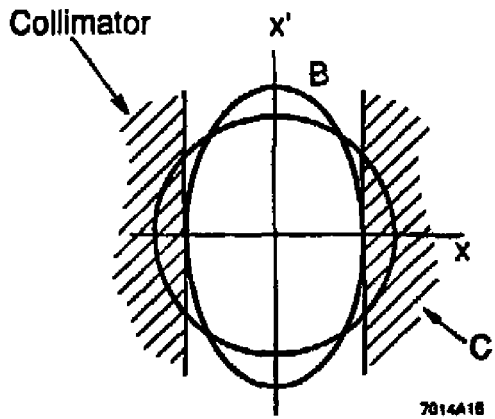

Figure 30 A collimator which cuts the position edges of a beam makes the beam have a new effective β and α, until filamentation restores them. The emittance of the beam is reduced until filamentation also restores it.

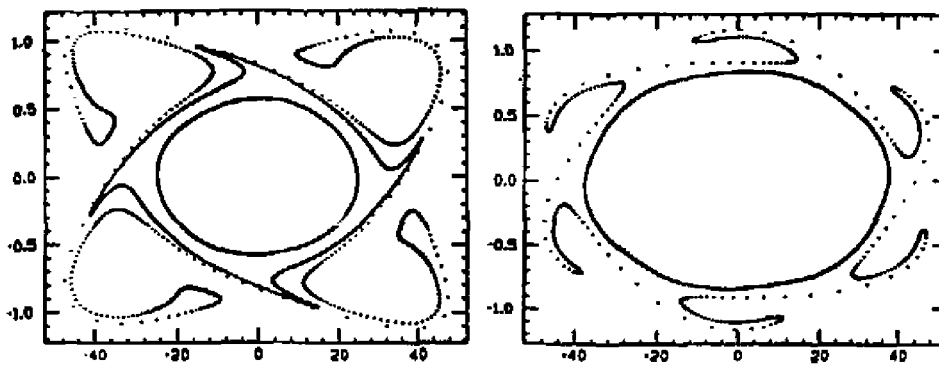

Figure 31 Nonlinear magnetic fields can distort phase space after many betatron oscillations. Here are shown two simulated phase space plots of a transport line (e^+ in the SLC) with 12 pole contributions to the quadrupoles. The left plot is for a 90 degree per cell lattice and the right plot is for 60 degrees per cell. Clearly, avoiding the natural resonance of the system (90 degrees per cell) is important for reducing phase space enlargement. Emittance measurements combined with simulations led to this discovery.

4.3 Profile Changes from Dispersion Errors

If mismatched, an initial dispersion in a transport line can increase the effective beam emittance immediately and increase the absolute emittance if allowed to filament. A view of the effective increase in emittance can be seen in Figure 32, where a dispersion η and the energy spread δ enter quadratically. Errors in η' also contribute. The measured effective emittance ε_{eff} in the presence of dispersion [27] is given by

$$\varepsilon_{eff}^2 = \varepsilon_\beta^2 + \frac{\varepsilon_\beta}{\beta_0}\left[\eta^2 + \left(\beta_0 \eta' + \alpha_0 \eta\right)^2\right]\left\langle \delta^2 \right\rangle \qquad (12)$$

and with filamentation the emittance increases further giving the final value of

$$\varepsilon_{eff} = \varepsilon_\beta + \frac{1}{2\beta_0}\left[\eta^2 + \left(\beta_0 \eta' + \alpha_0 \eta\right)^2\right]\left\langle \delta^2 \right\rangle. \qquad (13)$$

These effects have been measured in the SLC collider as shown in Figure 33. The errors in the dispersion on injection must be (and are) controlled to a few millimeters.

The presence of anomalous dispersion which affects the beam profile can also affect other routine measurements because it can not be distinguished from a normal betatron mismatch or another properly induced dispersion in the system. The effect on an energy spectrum measurement is shown in Figure 34.

5. TRANSVERSE PROFILE OSCILLATIONS AT HIGH CURRENTS

All effects discussed in Section 4 which affect the transverse beam profile are symmetrical, leaving the beam with left-right equality. Transverse wakefields are asymmetric and often produce skewed distributions. The oscillations shown in Figure 20 at high beam currents produce beam shapes similar to those shown in Figure 35 and 36. These distributions are not gaussian and must be described in a new way.

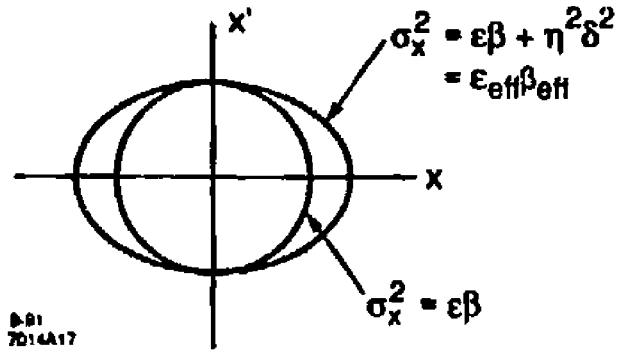

Figure 32 A dispersion mismatch η (η') combined with an energy spread δ produces an new effective emittance and β (α) of the beam. Standard emittance measurements obtain these effective parameters.

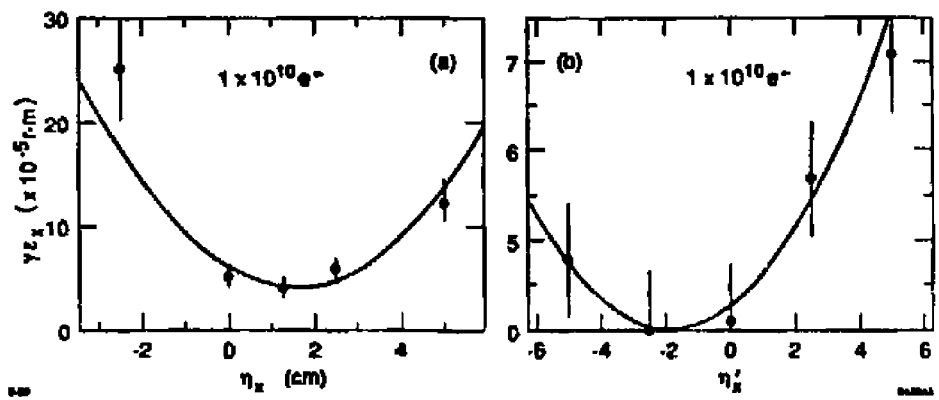

Figure 33 Emittance measurements at the end of the SLC accelerator as a function of dispersion errors at injection. The solid lines are theoretical predictions.

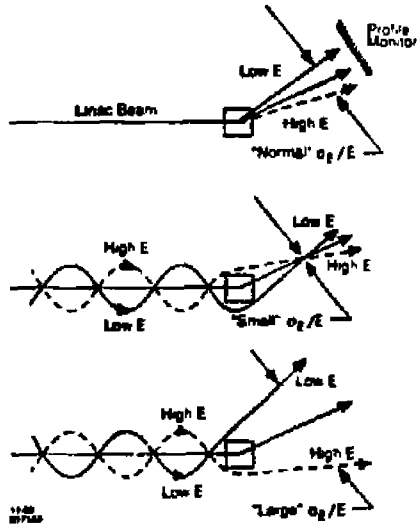

Figure 34a Measurement of the energy spread of the beam in a dispersion region at the end of the accelerator. Anomalous dispersion in the beam entering the spectrometer can effect the spectrum measurement.

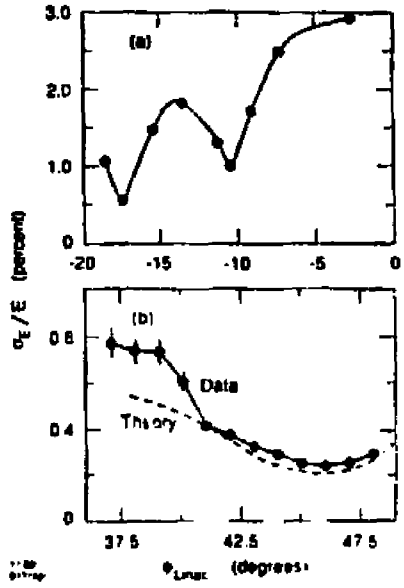

Figure 34b Measured energy spectrum as a function of the overall linac RF phase. The lower plot is for little anomalous dispersion in the beam. The upper plot has a sizable dispersion contamination. The apparent spectrum beats because the longitudinal phase of the dispersion in the linac is changed by the linac overall RF phase through the beam energy making the dispersion go in and out of phase with the planned dispersion in the spectrometer.

Figure 35 Images of an electron bunch on a profile monitor at 47 GeV showing wakefield growth with increasing oscillation amplitude. The left image is for a well steered beam. The center image is for an oscillation of about 0.5 mm and the right image for 1.0 mm. The bunch intensity is 2 X 10^{10} electrons. The core sizes are about 120 microns for x and y. Both horizontal and vertical oscillations are present.

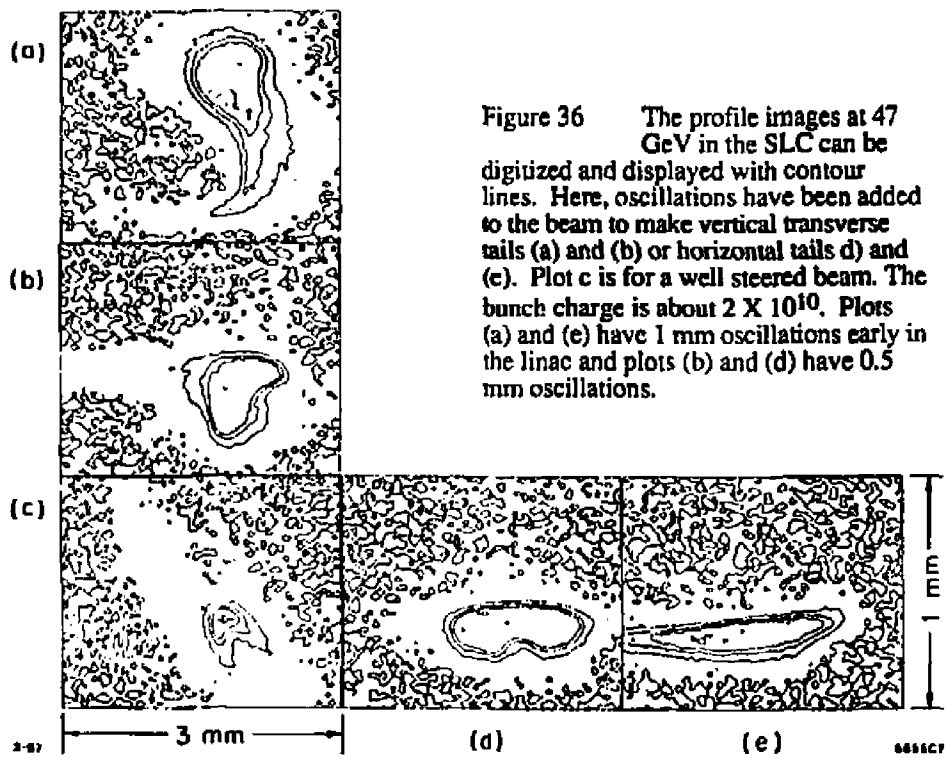

Figure 36 The profile images at 47 GeV in the SLC can be digitized and displayed with contour lines. Here, oscillations have been added to the beam to make vertical transverse tails (a) and (b) or horizontal tails d) and (e). Plot c is for a well steered beam. The bunch charge is about 2 X 10^{10}. Plots (a) and (e) have 1 mm oscillations early in the linac and plots (b) and (d) have 0.5 mm oscillations.

There have been several methods devised to quantify the beam core and transverse tail [28]. Multiple gaussian fits, skewness, kurtosis, and fitting left and right halves separately have been tried with various degrees of success.

An intuitive accelerator physics model for tail propagation is possible. A bunch executing a betatron oscillation in the quadrupole lattice of the linac experiences transverse wakefields in the accelerating structure. The head of the bunch drives the core and back of the bunch to ever increasing amplitudes producing a non-Gaussian tail. Simulations of this growth have been made where a bunch is divided into longitudinal slices and traced through the linac. A nearly exponential growth from head to back is apparent. The transverse particle distribution $\rho(x)$ of each slice is equal to that of the initial phase space distribution. The initial distribution for the SLC is a gaussian with width σ.

$$\rho(x) = \exp(- [x - x_0]^2 / 2\,\sigma^2) / \sigma\,(2\pi)^{1/2} \quad , \tag{14}$$

where x_0 is the mean of the distribution. The overall distribution must be integrated over the slices with different transverse positions x_0. The position x_0 of each slice is represented by an exponential which initiates at position z_0 along the length of the bunch and has a growth rate of τ. This tail rotates in phase space with the betatron phase ϕ_i but has an initial phase ϕ_0. The emittance of each slice of the beam is ε and the betatron function at each profile measurement 'i' is β_i. $\sigma_i^2 = \varepsilon\,\beta_i$. The tail extension is scaled locally by σ_i.

$$x_0(\phi_i, z) = \sigma_i\, U\,(z_0 - z)\,[\,\exp(\,(z_0 - z)\,\tau / \sigma_z) - 1\,]\,\cos(\phi_i + \phi_0) \tag{15}$$

where U is the unit step function and the bunch length is σ_z. The transverse distribution of each slice is given by :

$$\rho\,(x, \phi_i, z) = \exp(-\,(x - x_0(\phi_i, z))^2 / 2\sigma_i^2) / (2\,\pi)^{1/2}\sigma_i \tag{16}$$

Now, the overall transverse distribution we will call $f(x,\phi_i)$ is given by

$$f\,(x, \phi_i) = \int_{-\infty}^{+\infty} \rho\,(x, \phi_i, z)\, h\,(\,z\,)\, dz \tag{17}$$

where h(z) is the longitudinal profile, usually assumed to be a gaussian but with length σ_z. By choosing ϕ_0, τ, and z_0, the beam shape can be calculated at any location over a reasonably short region of the linac (less than a betatron wavelength so that wakefields do not change the distributions). Measured beam shapes can be analyzed to determine the tails structure of the beam and measure the effective ϕ_0, z_0, and τ. For a test, an oscillation was induced in the SLC electron beam with a dipole magnet and the resulting oscillation is shown in Figure 37a. The associated beam profiles on four wire scanners are shown in Figure 37b. The beam shapes observed have a definite tail with a particular phase. Various calculated beam shapes using the above formalism are shown in Figure 38. Clearly, many different shapes can be generated and these simulations can be easily matched to the observations.

6. OSCILLATION AND PROFILE TRANSVERSE JITTER

Time dependent changes in accelerator components can affect the beam in real time and produce pulse by pulse position shifts. Whereas in most studies averaging is used to reduce measurement noise, the study of beam jitter requires good single pulse measurement resolution. A typical pulse by pulse record of a beam position is shown in Figure 39 with its corresponding Fourier transform shown in Figure 40 [29]. If the data like that in Figure 39 is unacceptable, the source of the jitter must be found and eliminated (or a rapid feedback system built, see Section 7). The beam jitter itself may not be stable as it is likely to change at any moment, as can be seen in Figure 41. Measuring the beam jitter at many locations along the accelerator helps in isolating the source.

One method to improve the measurement resolution is to superimpose many beam pulses on one trajectory plot and look for correlations. One such display is shown in Figure 42 which indicates that the jitter occurs at a particular phase.

Another method to find the noise source is to make correlation plots between two variables in search of a common parameter. Figure 43 shows such a measured correlation between a beam position and intensity indicating a common problem (the damping ring RF in this case).

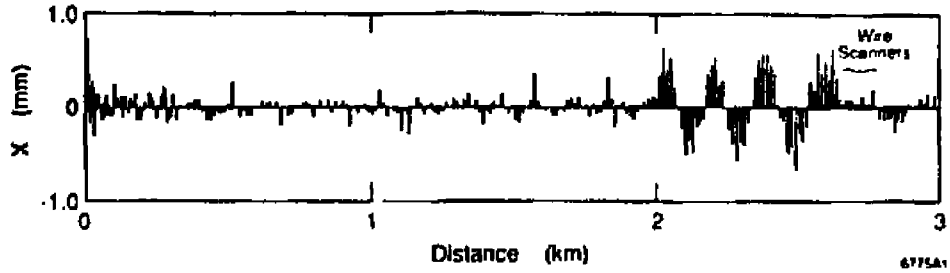

Figure 37a Induced horizontal oscillation of an SLC electron bunch which generates transverse tails from wakefields. σ_z = 1. mm and I⁻ = 3. X 10^{10} e⁻.

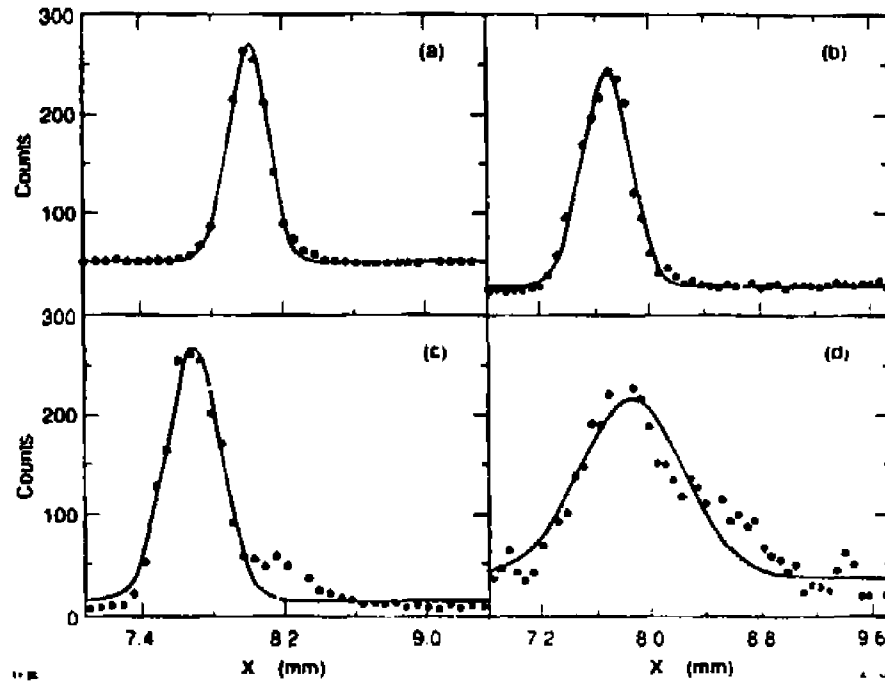

Figure 37b Measured beam profiles (47 GeV) for the betatron oscillation in Figure 37a. The projections were taken with four wire scanners spaced at (a) 0, (b) 22.5, (c) 90., and (d) 112.5 degrees in betatron phase. Note that the induced transverse tail has a particular phase such that the tail does not appear at position (a). The produced profiles have different shapes depending on the betatron phase. Consequently, the transverse tail rotates in phase space at the betatron frequency.

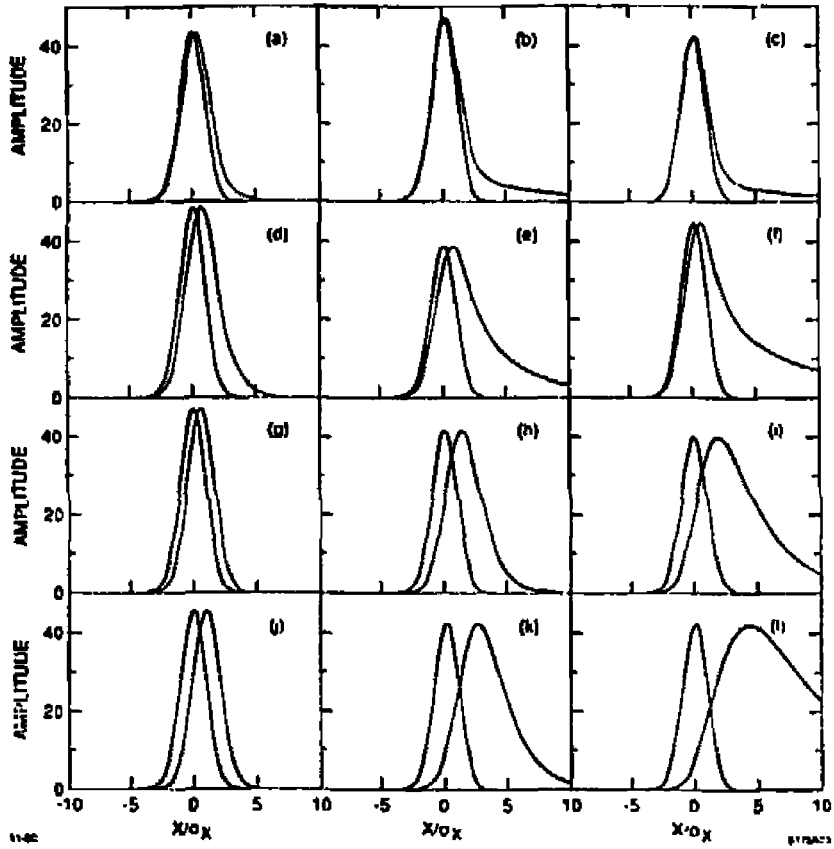

Figure 38 Calculated transverse bunch projections showing the effects of different input conditions with the rate of tail growth τ and the place z_0 along the bunch where the exponential growth starts. Large τ (horizontal axis) makes long thin tails and a z_0 closer to the front of the bunch (vertical axis) makes a broader shoulder.

Finally, the profile of the beam can also change with time as accelerator components drift (see Figure 44). These drifts are usually more difficult to identify as typically far fewer profile monitors are installed than position monitors because of their relative costs.

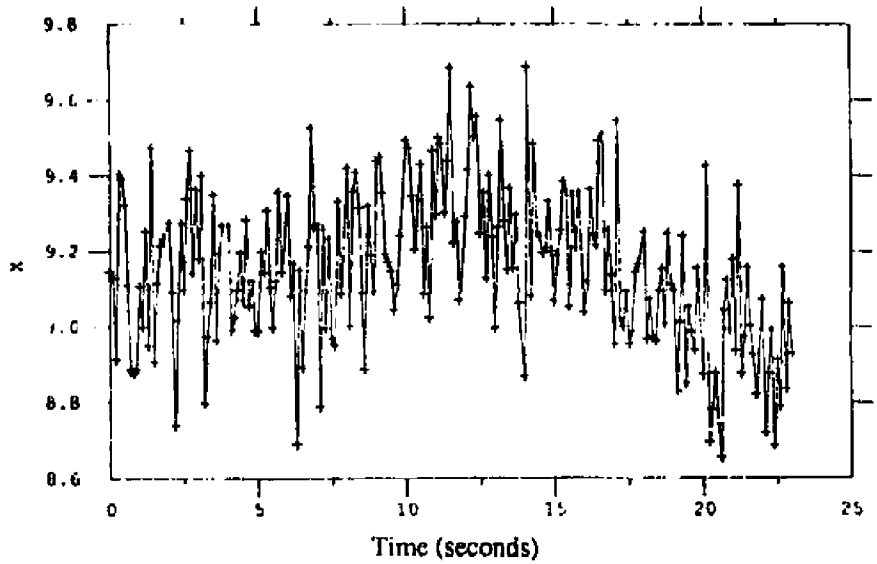

Figure 39 Measured beam position (mm) at one location (monitor) on every accelerator pulse as a function of time. Straight lines connect the data. Note the fast and slow drifts. A single position measurement has an error of about 20 microns.

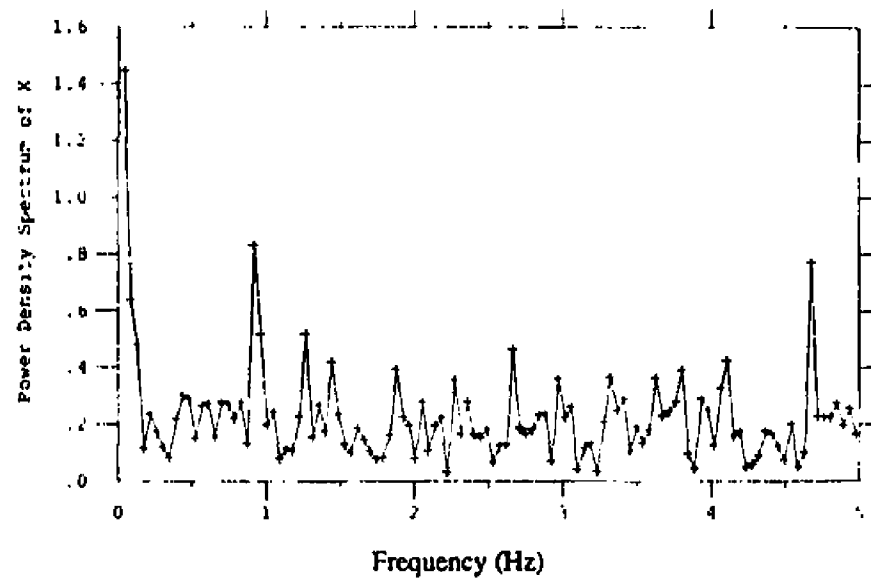

Figure 40 The Fourier transform of the data in Figure 39 showing white noise with additional power near 0 and 1 Hz.

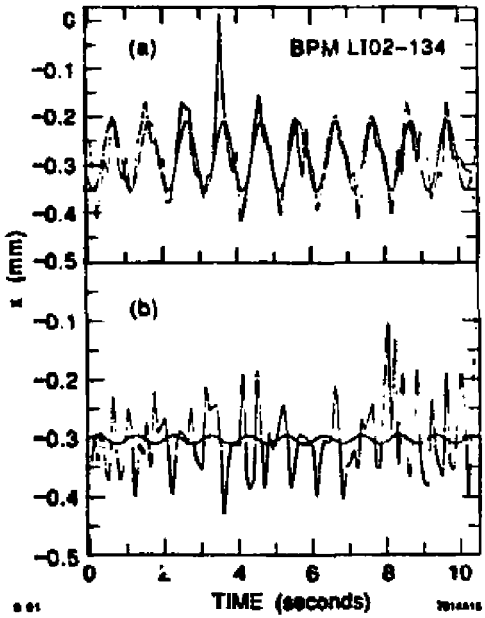

Figure 41 Measured bunch position as a function of time (straight lines) for two periods separated by 3 minutes. The sine curve is a fit to the data at 1.2 Hz. Note that the frequency spectrum of the beam jitter can change rapidly, even though the root-mean-square jitter is about the same.

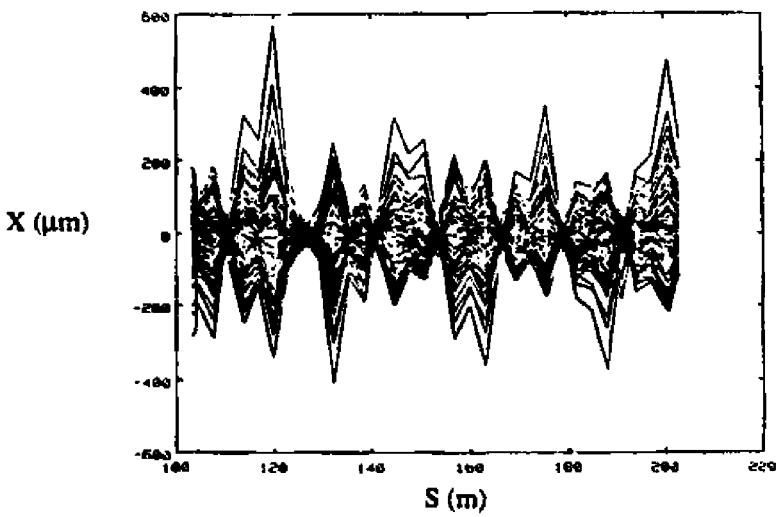

Figure 42 Measured single-pulse beam trajectories superimposed for multiple pulses. The amplitude of the position jitter changes with time but the phase of the oscillation is always the same. If the monitoring system is available, this envelope plot can be traced back to the jitter source. The relative position measurement errors from monitor to monitor can also be studied with this data.

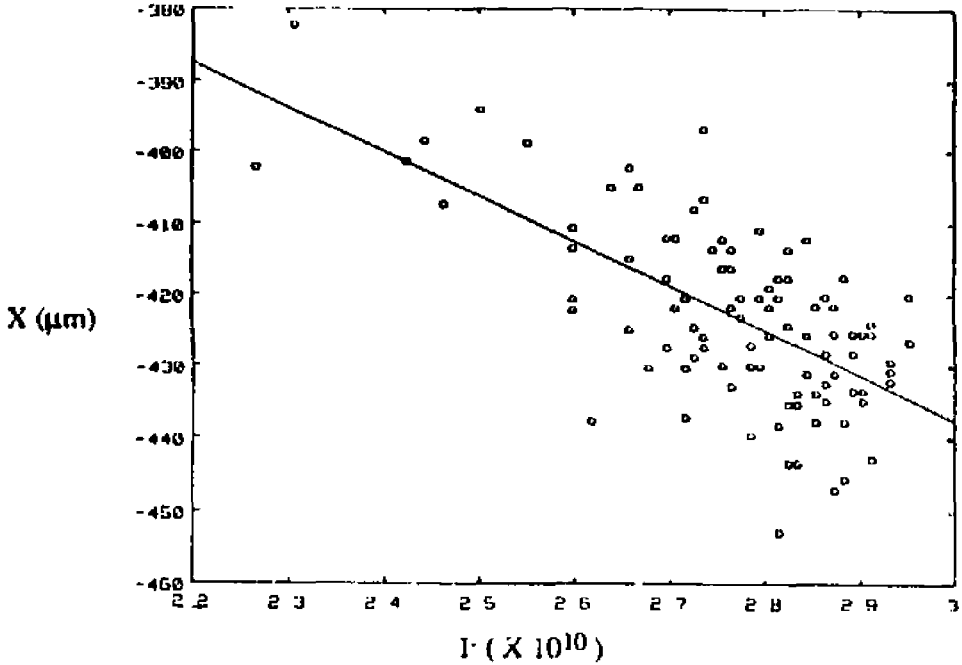

Figure 43 Measured correlation between the beam intensity and position.

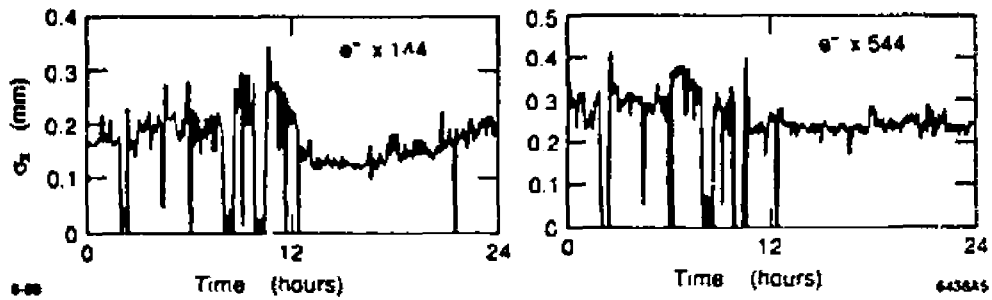

Figure 44 Measured bunch sizes as a function of time for two profile monitors located 90 degrees apart in betatron phase (47 GeV). Both the emittance and the betatron function of the beam are changing with time. Note that the time over which these beam parameters change is quite long.

7. FEEDBACK ON TRANVERSE OSCILLATIONS

Accelerators depend heavily on feedback systems to stabilize desired parameters. For example, the SLC has over 60 beam parameters under active feedback. The basic control equation for a position feedback is

$$\Delta\theta = \Delta x / R_{12} . \tag{18}$$

where Δx is the desired position change, R_{12} is the angle-to-position transport element between the dipole and position monitor, and $\Delta\theta$ is the required angle change of the beam. For angle and position feedback, a 2X2 transport matrix is needed. For angle and position feedback with both vertical and horizontal planes and with skew elements, a 4X4 matrix is needed. For two planes with skew and two beams (e^- and e^+), an 8X8 matrix is required. An example of a working feedback system for four electron beam parameters in the SLC is shown in Figure 45.

The data is sampled over a small region of the accelerator as in Figure 5a and is processed with modern control theory using weighting and filtering algorithms [30,31]. The frequency response of a typical feedback process in shown in Figure 46. The loop gain can not be less than unity at all frequencies. However, some adjustment of the gain profile is possible.

8. ACKNOWLEDGMENTS

The author wishes to thank many people at the Stanford Linear Accelerator Center and from other laboratories around the world for enlightening discussions about beam dynamics and observations. Special thanks are given to B. Richter, R. Littauer, P. Morton, J. Paterson, M. Ross, and J. Sheppard.

9. REFERENCES

1. G. Anger, Inverse Problems in Differential Equations, Plenum Press, 1988.
2. R. Erickson, ed.,"SLAC Linear Collider," December 1984.
3. J. Seeman, *Annu. Rev. Nucl. Part. Sci.* 41: 389-428 (1991).
4. K. Steffen, High Energy Beam Optics, John Wiley and Sons, New York, (1965).

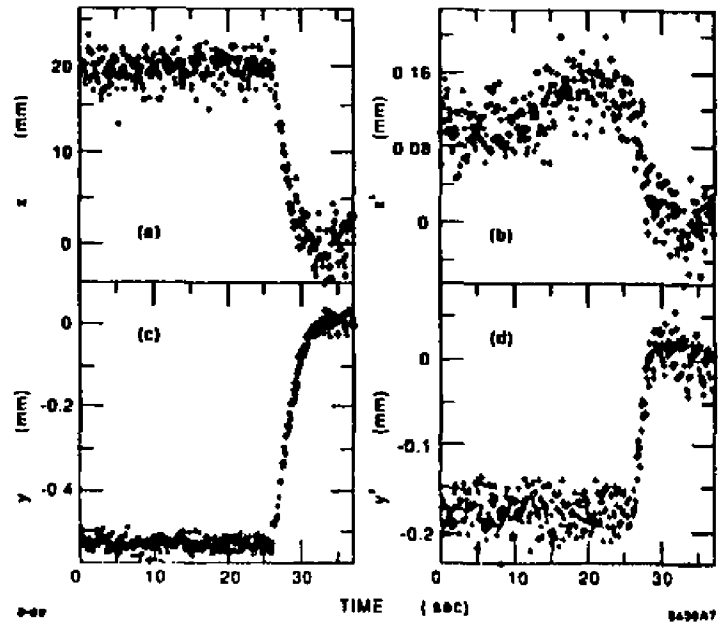

Figure 45 Measured response of the fast feedback process after turn on (at 26 seconds) operating at 10 hertz. x, x', y, and y' for a single beam are controlled simultaneously. Note that after the turn on of the feedback the high frequency noise is not damped and in certain cases larger.

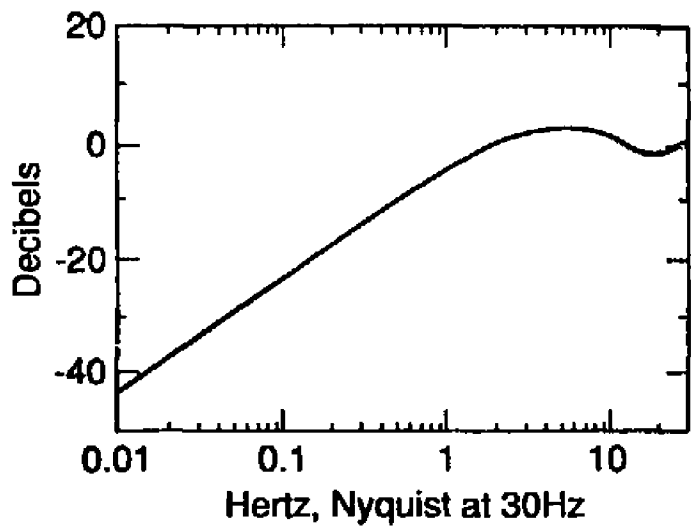

Figure 46 Theoretical frequency response of a typical feedback loop using an exponential weighting of about 6 pulses. Below 2 Hz the disturbances are damped. Above 2 Hz the disturbances are amplified. Control of the filtering and weighting of the data can alter this response to damp noise at higher frequencies at the expense of damping at lower frequencies.

5. K. Brown, F. Rothacker, D. Carey, and C. Iselin, SLAC Report-91 Rev.2 (1977).
6. K. Brown, SLAC Report-75, (1982).
7. C. Bovet, R. Gouiran, I. Gumowski, K. Reich, CERN/MPS-SI/ DL/70/4 (1970).
8. J. Laclare, Proc. of 11th Int. Conf. on High Energy Accelerators, p. 526 (1980).
9. R. Littauer, "Beam Instrumentation," AIP Conf. Proc.# 105, p. 869 (1983).
10. R. Siemann, 'Bunched Beam Diagnostics', AIP Conf. Proc. #184, p. 430 (1989).
11. M Sands, "The Physics of Electron Storage Rings," SLAC Report 121 (1970).
12. T. Himel and K. Thompson, SLAC-PUB-4917 (1989).
13. M. Lee, et al., SLAC-PUB-4540 (1988).
14. J. Seeman and J. Sheppard, SLAC-PUB-4421 (1987).
15. P. Emma, SLAC CN-381 (1990).
16. J. Seeman, et al., SLAC-PUB-3945 (1986).
17. J. Seeman, et al., SLAC-PUB-5438 (1991).
18. T. Raubenheimer, SLAC-PUB-5355 (1990).
19. V. Balkin, et al., 12th Int. Conf. on High Energy Acc., FNAL, p. 119 (1983).
20. C. Adolphsen, et al, SLAC-PUB-5581 (1991).
21. M. Ross, SLAC-PUB-3640 (1985).
22. M. Ross, et al., SLAC-PUB-5556 (1991).
23. M. Ross, et al., SLAC-PUB-4278 (1987).
24. J. Seeman, et al., SLAC-PUB-5437 (1991)
25. W. Spence, unpublished.
26. H. Braun, et al., SLAC SLC Experimental Note 144 (1990).
27. L. Mermings, et al., SLAC-PUB-5514 (1991).
28. J. Seeman, et al., SLAC-PUB-5440 (1991).
29. J. Seeman, SLAC SLC Experimental Note 249 (1991).
30. R. Stiening, SLAC CN-14 (1980).
31. T. Himel, et al., SLAC-PUB-5470 (1991).

DISCLAIMER